Available online at www.sciencedirect.com
SCIENCE DIRECT®
ELSEVIER
International Journal of Solids and Structures 43 (2006) 1189–1200
INTERNATIONAL JOURNAL OF SOLIDS and STRUCTURES
www.elsevier.com/locate/ijsolstr

Fracture investigation at V-notch tip using coherent gradient sensing (CGS)

X.F. Yao [a,*], H.Y. Yeh [b], W. Xu [a]

[a] Department of Engineering Mechanics, FML, Tsinghua University, Qinghua Yuan, Hai Dian District, Beijing 100084, China
[b] Department of Mechanical and Aerospace Engineering, California State University, Long Beach, CA 90840-8305, USA

Received 4 November 2004; received in revised form 11 March 2005
Available online 19 April 2005

Abstract

Local deformation field and fracture characterization of mode I V-notch tip are studied using coherent gradient sensing (CGS). First, the governing equations that relate to the CGS measurements and the elastic solution at mode I V-notch tip are derived in terms of the stress intensity factor, material constant, notch angle and fringe order. Then, a series of CGS fringe patterns of mode I V-notch are simulated, and the effects of the notch angle on the shape and size of CGS fringe pattern are analyzed. Finally, the local deformation field and fracture characterization of mode I V-notch tip with different V-notch angles are experimentally investigated using three-point-bending specimen via CGS method. The CGS interference fringe patterns obtained from experiments and simulations show a good agreement. The stress intensity factor obtained from CGS measurements shows a good agreement with finite element results under K-dominant assumption.

Keywords: V-notch; Coherent gradient sensing; Stress intensity factor; Fracture

1. Introduction

As a kind of geometrical discontinuity, V-notch frequently encounters in engineering structures. V-notch usually acts as a singular stress concentrator, which has a direct relation with notch geometrical configuration (i.e. notch angle, the radius of notch tip) and material constant. In reality, this kind of stress singularity easily initiates fracture and crack propagation. Therefore, it is important to study the stress singularity and fracture character at the V-notch tip.

* Corresponding author. Tel.: +86 10 62771546; fax: +86 10 62771113.
E-mail address: yxf@mail.tsinghua.edu.cn (X.F. Yao).

0020-7683/$ - see front matter
doi:10.1016/j.ijsolstr.2005.03.043

Most studies so far of V-notch singular field are concentrated on the theoretical analysis and numerical approaches. Williams (1952) first studied the V-notch problem for linear elastic bodies and described the singular stress field using eigenfunction approach. Atkinson et al. (1988) derived a path independent integral for calculating stress intensity factor at V-notches. Chen (1995) studied the notch stress intensity factor for single and double edge notch strip using body force method. Dunn et al. (1997) studied the fracture initiation at sharp notches using critical stress intensities.

However, only a few works about the stress singularity and fracture characterization at V-notch tip have been studied and reported by experimental community. Prassianakis and Theocaris (1990) extracted the stress intensity factor for V-notched elastic, symmetrically loaded plates using the method of caustics. Mahinfalah and Zackery (1995) studied stress singular field for sharp reentrant corners using photoelastic technology. Kondo et al. (2001) determined the stress intensities of sharp-notched strips using strain gage method. But these methods have some inherent shortcomings in practical application, such as the limitations of birefraction material for photoelasticity, local field of caustic (Xu et al., 2004; Yao et al., 2004a; Yao et al., 2004b) and the so-called "point measurement" of strain gage technology (Yao et al., 2003).

Coherent gradient sensing (CGS) is double grating lateral-shearing interferometric technique with the simplicity of the optical setup, non-contact, real-time, full-field optical information and variable resolution, which has shown many applications in the study of quasi-static as well as dynamic crack-tip field in both homogeneous and composite materials. It can be used both in a reflection mode (for opaque materials) and in a transmission mode (for transparent materials). The physical principle of the CGS is that the fringe pattern on the image plane by the interference of the shifted and unshifted beams is related to the spatial difference of the phase in the shearing direction, which represents a locus of equal gradient component of the phase. Tippur et al. (1992) and Tippur and Xu (1995) first developed the lateral-shearing interferometric technique of CGS to study the crack-tip deformations in transparent and opaque materials. Lee et al. (1996) established the relation between the optical path difference and the deformation or stress field for the reflected or transmitted coherent laser beam from a deformed plate specimen by the precise analysis of CGS technology based on Fourier optics. Lambros and Rosakis (1997) obtained real-time interferograms of the near-tip deformation during dynamic crack initiation and propagation by the optical experiments on dynamically deformed thick polymeric-composite laminated plates. Rosakis et al. (1998) measured the curvature and curvature changes in thin film deposited on silicon wafers and micro-mechanical structures using CGS. Park et al. (2003) investigated large deformation behavior prior to and after the bifurcation of thin W films on much thicker Si substrates using CGS. El-Hadek and Tippur (2003a) and El-Hadek and Tippur (2003b) studied the mode I crack initiation and growth behaviors on functionally graded syntactic foam sheets under low velocity impact loading using reflection CGS technique and high-speed photography.

In this paper, CGS method with the transmission mode is used to study the stress singularity and fracture behaviors at the V-notch tip. Numerical simulations of the optical effect for the material with different notch angles are performed. The corresponding CGS experiments in three-point-bending specimen with different V-notches are presented. The stress intensity factors at mode I V-notch tip are obtained by the least-squares analysis. The influences of different V-notches on fracture characterizations are compared and analyzed.

2. Elastic singular stress field at the V-notch tip

For the V-notch subjected to plane stress state in an isotropic solid in Fig. 1, the elastic singular stress field in the vicinity of the notch tip is expressed as (Williams, 1952; Seweryn and Molski, 1996)

$$\sigma_r = \frac{K_I}{(2\pi r)^{1-\lambda} C_1}\left[\frac{3-\lambda}{1+\lambda}\cos(1+\lambda)\alpha\cos(1-\lambda)\theta + \cos(1-\lambda)\alpha\cos(1+\lambda)\theta\right], \tag{1}$$

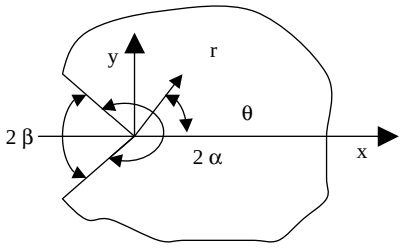

Fig. 1. Geometrical configuration at the V-notch tip.

$$\sigma_\theta = \frac{K_I}{(2\pi r)^{1-\lambda} C_1}[\cos(1+\lambda)\alpha\cos(1-\lambda)\theta - \cos(1-\lambda)\alpha\cos(1+\lambda)\theta], \tag{2}$$

$$\sigma_{r\theta} = \frac{K_I}{(2\pi r)^{1-\lambda} C_1}\left[\frac{1-\lambda}{1+\lambda}\cos(1+\lambda)\alpha\cos(1-\lambda)\theta - \cos(1-\lambda)\alpha\cos(1+\lambda)\theta\right]. \tag{3}$$

With

$$C_1 = \cos(1+\lambda)\alpha - \cos(1-\lambda)\alpha, \quad \alpha = \pi - \beta.$$

Here 2β is the angle of V-notch, (r,θ) is the polar coordinates with respect to V-notch tip. K_I is the stress intensity factor at the apex of the wedge. For the V-notch tip, the stress intensity factor is not the function of $r^{-1/2}$, but $r^{\lambda-1}$, because K_I in the Eqs. (1)–(3) can be defined as

$$K_I = \left.\frac{\sigma_\theta}{(2\pi r)^{\lambda-1}}\right|_{(\theta=0)}, \tag{4}$$

where the unit of K_I is MPa $m^{1-\lambda}$. λ is the order of singularity which depends on the notch angle, and can be expressed as

$$\lambda\sin 2\alpha + \sin 2\lambda\alpha = 0. \tag{5}$$

The values of λ for the different notch angle 2β are summarized in Table 1.

3. Application of the CGS technique to V-notch stress analysis

3.1. Basic principles of CGS technology

The CGS is a new full field and lateral-shearing interferometric technique. Governing equations of CGS were first analyzed and described by Tippur et al. (1992), Tippur and Xu (1995), Rosakis (1993) and Bruck and Rosakis (1992, 1993). It is sensitive to gradient of deformations in the optical path. In transmission mode these deformation gradients are due to refractive index changes of the specimen induced by stress gradient. The basic governing equation of transmission CGS is

Table 1
The values of λ for different notch angle 2β

2β	0°	30°	60°	90°	120°	150°
2α	360°	330°	300°	270°	240°	210°
λ	0.5	0.5014	0.5123	0.5445	0.6157	0.7520

$$x\text{-direction: } ch\frac{\partial(\widetilde{\sigma}_x+\widetilde{\sigma}_y)}{\partial x}=\frac{mp}{\Delta}\quad m=0,\pm1,\pm2,\ldots \tag{6}$$

$$y\text{-direction: } ch\frac{\partial(\widetilde{\sigma}_x+\widetilde{\sigma}_y)}{\partial y}=\frac{np}{\Delta}\quad n=0,\pm1,\pm2,\ldots \tag{7}$$

where p and Δ are the pitch and separation of the two high-density gratings. m and n are the fringe orders for the x and y gradient contours, respectively. c is stress optical constant of the material and h is the thickness of the specimen. $\widetilde{\sigma}_x$ and $\widetilde{\sigma}_y$ are through-thickness average of normal stress components. CGS fringes provide the gradient of $(\widetilde{\sigma}_x+\widetilde{\sigma}_y)$ in the x- and y-direction, respectively.

3.2. Governing equations at V-notch tip using CGS technology

From elastic stress field (Eqs. (1)–(3)) for V-notch, the sum of in-plane principal stresses is expressed as

$$\widetilde{\sigma}_x+\widetilde{\sigma}_y=\frac{4K_{\mathrm{I}}}{(2\pi r)^{1-\lambda}(1+\lambda)C_1}\cos[(1+\lambda)\alpha]\cos[(1-\lambda)\theta]. \tag{8}$$

In the analysis of CGS, the orientation of two high-density gratings is selected to be perpendicular to the crack orientation. Stress gradient contours in the x-direction can be described by combining Eq. (6) with Eq. (8) in the following form:

$$ch\frac{\partial(\widetilde{\sigma}_x+\widetilde{\sigma}_y)}{\partial x}=-\frac{2^{\lambda}ch\pi^{-1+\lambda}r^{-2+\lambda}(-1+\lambda)\cos[(-2+\lambda)\theta]\cos[(1+\lambda)\alpha]\csc\alpha\csc(\lambda\alpha)}{1+\lambda}K_{\mathrm{I}}=\frac{mp}{\Delta}. \tag{9}$$

From Eq. (9), the mode I stress intensity factor at V-notch tip can be expressed as

$$K_{\mathrm{I}}=\frac{mp}{ch\Delta}\frac{1+\lambda}{2^{\lambda}\pi^{\lambda-1}(1-\lambda)\cos[(1+\lambda)\alpha]\csc\alpha\csc\lambda\alpha}\frac{1}{r^{\lambda-2}\cos[(\lambda-2)\theta]}. \tag{10}$$

Once the fringes are digitized, the stress intensity factors can be calculated by using Eq. (10).

It should be pointed out that the Eq. (10) cannot be directly used for sharp crack because $C_1=0$ for $2\beta=0^\circ$. Limiting values for σ_r and σ_θ can be obtained as

$$\lim_{\alpha\to\pi}\widetilde{\sigma}_r=\frac{K_{\mathrm{I}}}{\sqrt{2\pi r}}\frac{1}{4}\left(5\cos\frac{\theta}{2}-\cos\frac{3\theta}{2}\right)\qquad\lim_{\alpha\to\pi}\widetilde{\sigma}_\theta=\frac{K_{\mathrm{I}}}{\sqrt{2\pi r}}\frac{1}{4}\left(3\cos\frac{\theta}{2}+\cos\frac{3\theta}{2}\right). \tag{11}$$

Hence K_{I} for mode I crack can be expressed as

$$K_{\mathrm{I}}=-\frac{\sqrt{2\pi}mp}{ch\Delta}\frac{r^{3/2}}{\cos(3\theta/2)}. \tag{12}$$

3.3. Numerically simulated CGS fringes surrounding the V-notch tip

According to the governing Eq. (9), the CGS fringes around the mode I V-notch tip can be simulated based on the K-dominant assumption. Fig. 2 shows the CGS fringes around the V-notch tip corresponding to the constant stress intensity factor $K_{\mathrm{I}}=1$ MPa $\mathrm{m}^{1-\lambda}$, and the notch angle $2\beta=0^\circ$, 30°, 60°, 90°, 120°, 150° respectively. Because the orientation of the two high-density gratings line is assumed to be perpendicular to the crack in this simulation, the CGS fringes are loci of constant slope $\partial(\widetilde{\sigma}_x+\widetilde{\sigma}_y)/\partial x$.

From Fig. 2 it can be seen that CGS fringe patterns at V-notch tip consist of three parts: the front loops, the left and the right loops. The left and right loops are symmetric with respect to the line dividing notch angle into two halves. The front loops of CGS fringe patterns at V-notch tip have the similar geometrical

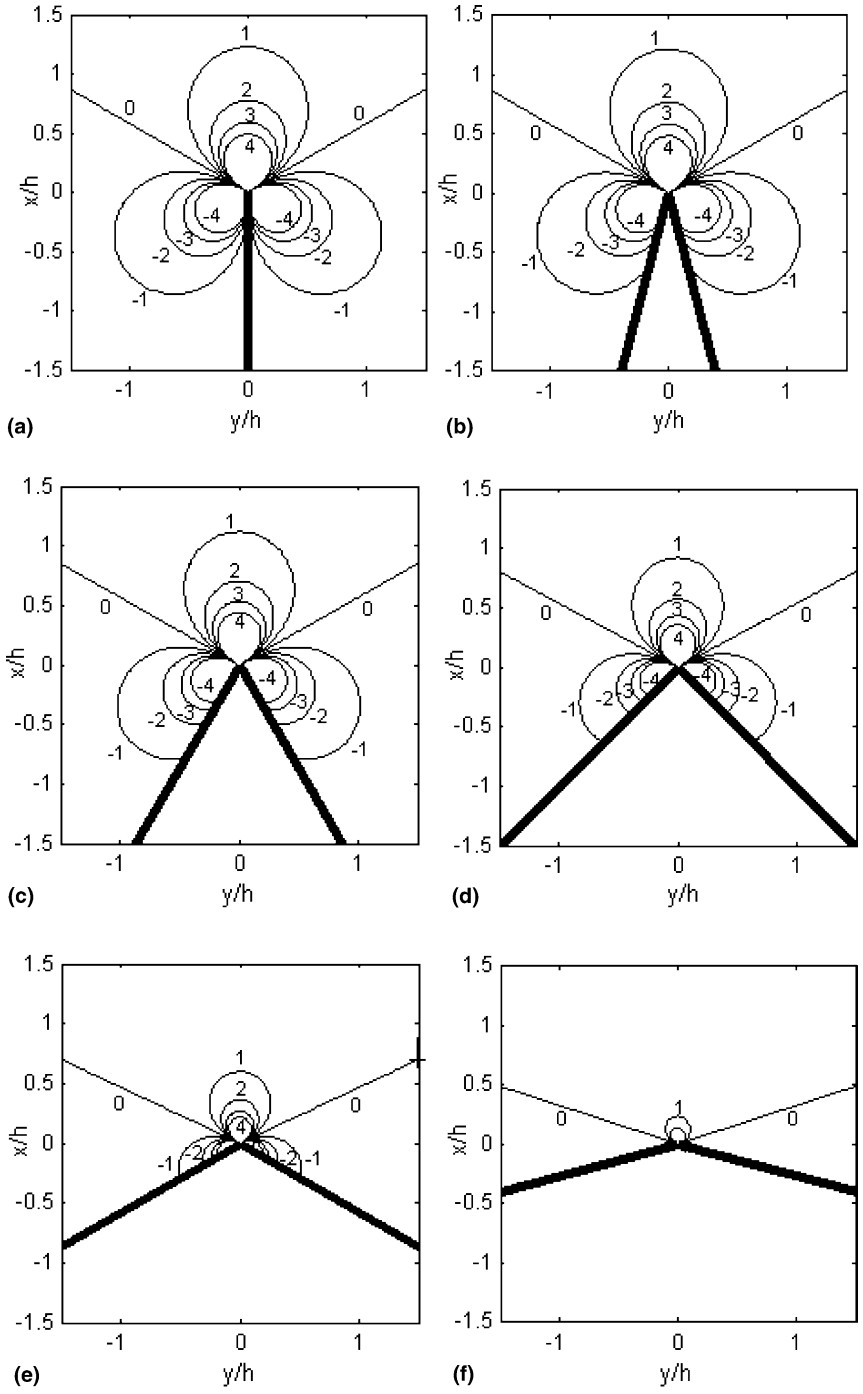

Fig. 2. Numerical modeling of CGS fringe patterns at the V-notch tip ($K_I = 1$ MPa $m^{1-\lambda}$): (a) $2\beta = 0°$; (b) $2\beta = 30°$; (c) $2\beta = 60°$; (d) $2\beta = 90°$; (e) $2\beta = 120°$; (f) $2\beta = 150°$.

configuration for different notch angles, but the geometrical patterns of the left and right lobes are influenced by the V-notch boundary. With the same magnitude of stress intensity factor and the same optical setup, the larger the V-notch angle is, the smaller three fringe loops are. Therefore the CGS fringe patterns at mode I crack tip with $2\beta = 0°$ is the largest. When the notch angle is large enough, the left and right lobes almost disappear and the front loops existed solely. This phenomenon lies in the rapid diminishing of deformation gradient at the left and right edge around the notch tip with the larger notch angle. It is noticed that the fringes of integer number is a bright fringe in the practical experiment.

4. CGS measurement of stress intensity factor at the V-notch tip

From Eqs. (10) and (12), stress intensity factor at the V-notch tip can be determined.

4.1. PMMA specimen with V-notch

Three-point-bending PMMA specimen with the nominal geometrical dimensions 110 mm × 40 mm × 4 mm is used as shown in Fig. 3. Six specimens with the V-notch were carefully prepared using a special machine tool for the same notch depth 10 mm and different notch angles $2\beta = 0°$, 30°, 60°, 90°, 120°, 150°. The material properties and stress optical constant of the PMMA specimen are listed in Table 2.

4.2. CGS setup

The optical setup of CGS method in transmission mode is shown in Fig. 4. First, a coherent laser beam with wavelength 632 nm was expanded and collimated to obtain a beam 150 mm in diameter that was centered at initial notch tip of the specimen. The incident object wavefronts transmitted through a pair of identical high-density Ronchi grating (40 lines/mm) G_1 and G_2 separated by a distance $\Delta = 50$ mm. The grating lines perpendicular to the notch central line have been chosen in order to obtain the x-direction gradient information of the notch-tip stress fields. Finally, the diffracted wavefronts from the two gratings are spatially filtered using a filter lens to form distinct diffraction spots on the filter plane. A filtering aperture is placed in this plane in order to filter out the +1 or −1 diffraction order of interest and reject other orders.

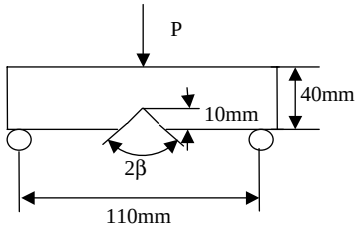

Fig. 3. PMMA specimen with V-notch ($2\beta = 0°, 30°, 60°, 90°, 120°, 150°$).

Table 2
The material properties of the PMMA specimen

Material	PMMA
Elastic modulus E (GPa)	3.24
Poisson's ratio v	0.35
Stress optical constant c (m^2/N)	-1.08×10^{-10}

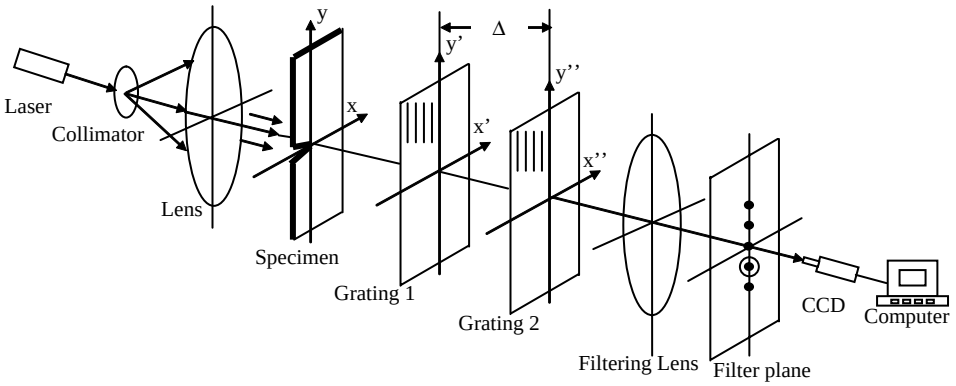

Fig. 4. CGS optical setup in transmission.

The filtered beam of interest is then further imaged onto the focal plane of a CCD camera. The video image is digitized and processed to extract the deformation gradient information on the specimen.

In the current CGS optical setup, the fringe sensitivity, S, is pitch p over grating distance Δ, and $S = \frac{p}{\Delta}$ is 0.0005°/fringe.

4.3. Analysis of CGS fringe patterns at V-notch tip

The CGS experiments of V-notch in three-point-bending PMMA specimen are carried out, the load cell was used to measure the applied load. Fig. 5 shows typical CGS fringe patterns at V-notch tip with loading level $P = 200$ N for notch angle $2\beta = 0°$, 60°, 120°, respectively. The black real line is numerically synthesized using K_I extracted from the fringe patterns based on the K-dominance assumption. By superimposing experimental and theoretical fringes in Fig. 5, it can be seen that the front loops of CGS fringe patterns at V-notch tip show a good agreement, and the geometrical patterns of the left and right loops are not in good agreement with theoretical contours. This phenomenon lies in two reasons: (a) superposition of the stresses due to loading and the residual stresses due to V-notch boundary machine cutting; (b) the variation in notch tip triaxiality with notch angle. In Fig. 5, the dash lines represent the inner and outer boundaries of the K-dominance zone ($0.5 \leqslant r/h \leqslant 1.25$), it can be seen that there is a good agreement between the

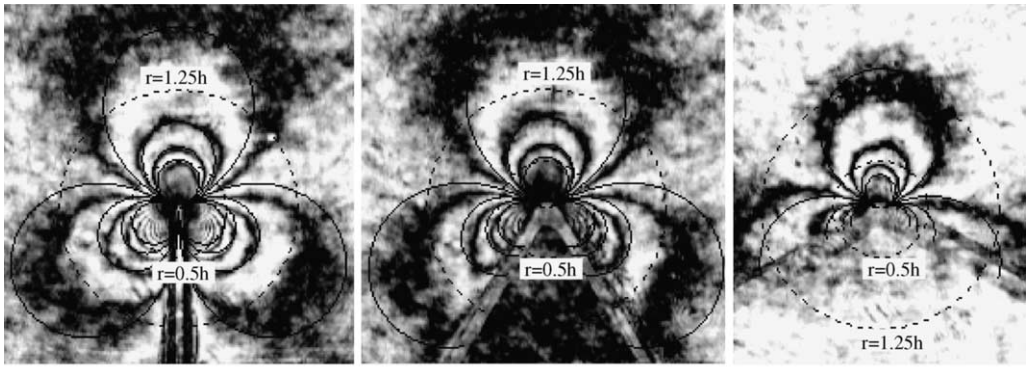

Fig. 5. Experimental and simulated CGS fringe pattern at the V-notch tip ($P = 200$ N): $2\beta = 0°$, $2\beta = 60°$, $2\beta = 120°$.

experiment and the analysis within the K-dominance zone, the only differences appeared in the region of $r < 0.5h$ and $r > 1.25h$. Therefore the K-dominance region should be selected within the front loops of CGS fringe.

For the CGS fracture experiment of each notched specimen, the stress field near V-notch tip is continuously reinforced and the CGS fringe loops are also enlarged continuously with the increased applied load.

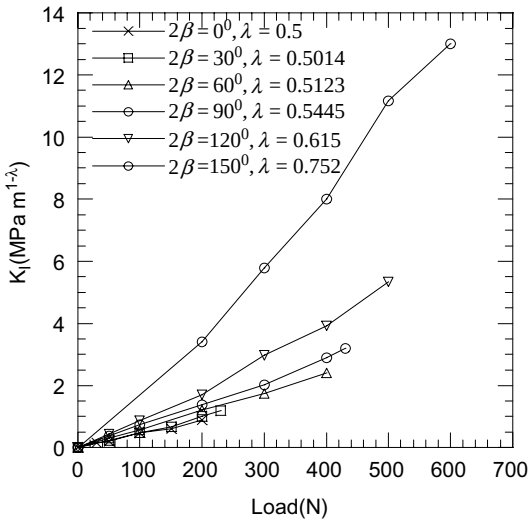

Fig. 6. Stress intensity factor at the V-notch tip.

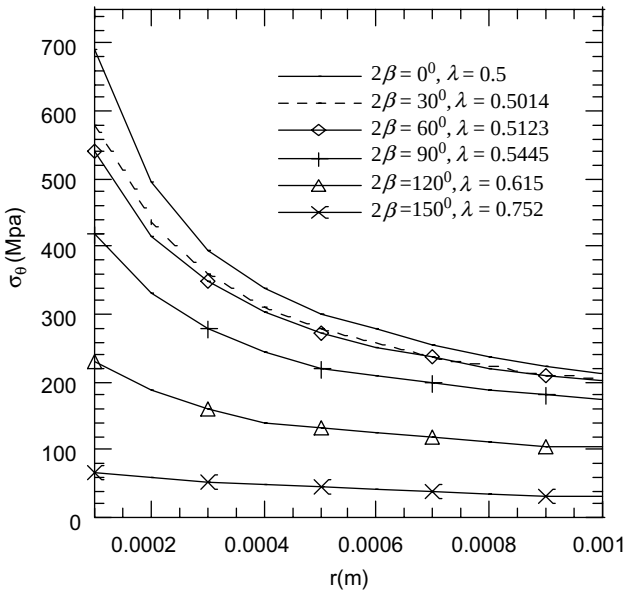

Fig. 7. σ_θ along $\theta = 0°$ at $P = 100$ N.

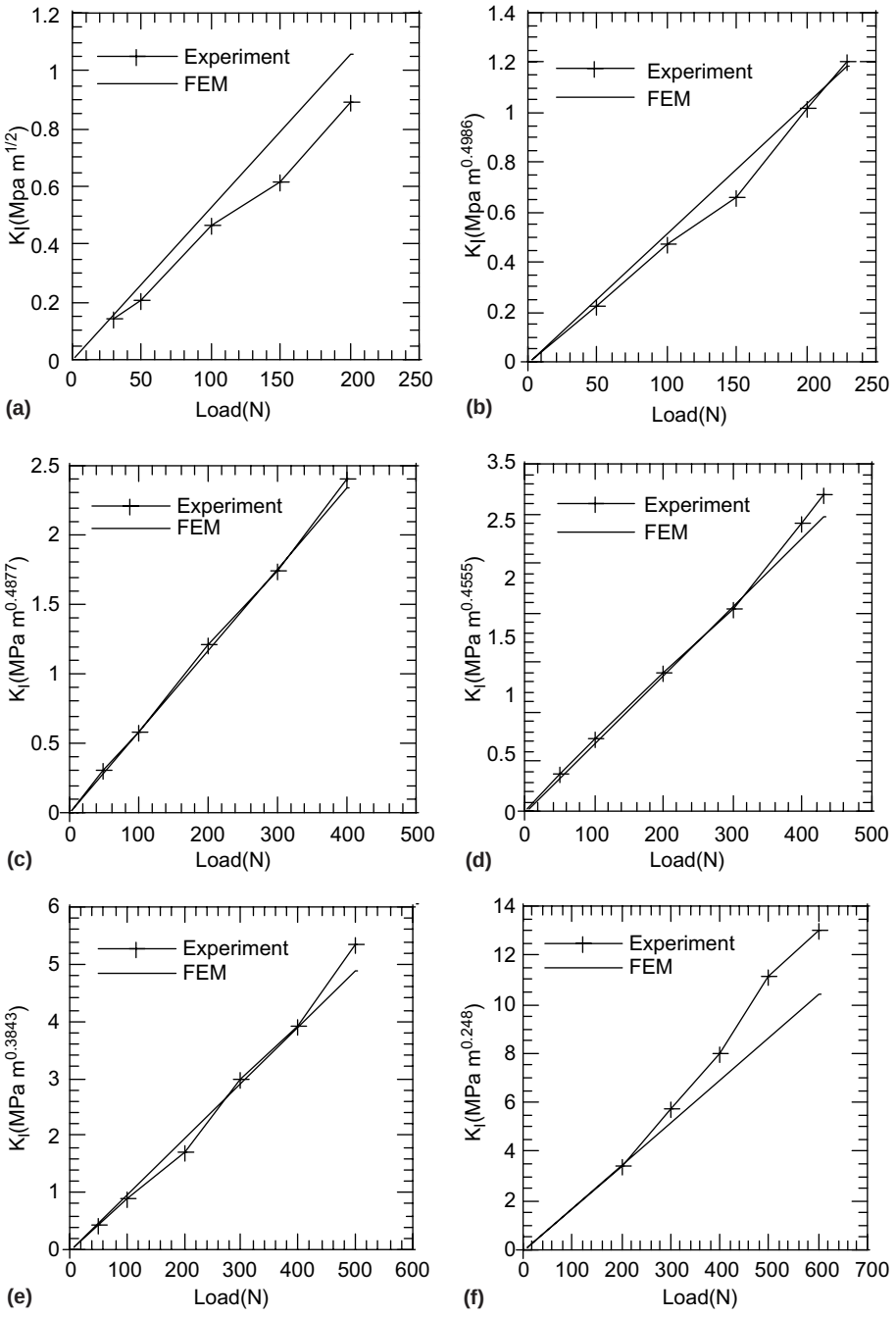

Fig. 8. The stress intensity factor comparison—experiment vs FEM: (a) $2\beta = 0°$; (b) $2\beta = 30°$; (c) $2\beta = 60°$; (d) $2\beta = 90°$; (e) $2\beta = 120°$; (f) $2\beta = 150°$.

In order to extract the mode I stress intensity factor at V-notch tip, the CGS fringe patterns at V-notch tip is digitized to analyze and get the fringe order m and location (r,θ) with respect to the notch tip. Eq. (10) can be expressed as

$$K_{\mathrm{I}} = \frac{mp}{ch\Delta}\frac{1+\lambda}{2^{\lambda}\pi^{\lambda-1}(1-\lambda)\cos[(1+\lambda)\alpha]\csc\alpha\csc\lambda\alpha}\frac{1}{r^{\lambda-2}\cos[(\lambda-2)\theta]} = Y(r,\theta,m). \tag{13}$$

Here $Y(r,\theta,m)$ can be retrieved from digitized experimental data r_i, θ_i, m_i $(i=1,\ldots,N)$ of CGS fringes, which is a constant and is the same as the mode I stress intensity factor. From the analysis of Rosakis and Ravi-Chandar (1986) and Krishnaswamy et al. (1992), data points must be chosen at a distance from the notch tip greater than half of the specimen thickness to avoid the influence of three-dimensional effects. In this paper, the K-dominance region exists for $0.5 < r/h < 1.25$ and $-60^\circ < \theta < 60^\circ$.

Fig. 6 shows the variation of K_{I} for various notch angles. It is noticed that under the same loading condition the larger the notch angle 2β, the larger the stress intensity factor is. But it does not imply higher stress concentration for the larger notch angle. The main reason is that the unit of the stress intensity factor is different for various 2β values (as shown in Eq. (4), for V-notch tip, the stress intensity factor is not the function of $r^{-1/2}$ but $r^{\lambda-1}$, and λ depends on the notch angle). In order to compare the stress singularity under the same loading with different 2β value, Fig. 7 gives the trend of σ_θ along the line of $\theta = 0^\circ$ at $P = 100$ N, where σ_θ is calculated using Eq. (2). From Fig. 7, it can be seen that the trend of stress concentration depends on the 2β value. Smaller the 2β value will develop the higher stress concentration.

4.4. K_I comparison—experiment vs finite element method

Stress intensity factor at the V-notch tip is also obtained via J-integral using the finite element method (FEM). Here, the commercial calculating software of ABAQUS is used, three-dimensional tetrahedron elements are selected for the notch tip region and three-dimensional hexahedral elements are used for the rest parts. The mesh size is very small and the total elements used are 70,000. From Fig. 8 it can be seen that the stress intensity factor obtained from the CGS experiment and the numerical calculation matches quite well. This suggests that the CGS technology is very effective for studying the V-notch fracture behavior.

5. Conclusions

Local deformation field and fracture characterization at mode I V-notch tip are experimentally investigated using CGS and numerically simulated by FEM. Following are the conclusion from current study:

(1) The CGS governing equations at the mode I for V-notch tip are established, correlating stress intensity factor, material constant, notch angle, fringe order, etc.
(2) CGS fringe patterns at V-notch tip consist of three parts: the front loops, the left and the right loops. The left and right loops are symmetric with respect to the line dividing notch angle into two halves. The front loops have the similar geometrical configuration for different notch angles, but the geometrical patterns of the left and right loops are influenced by V-notch boundary, and display the deformation gradient information surrounding the notch tip.
(3) The influences of the notch angle on the shape and size of CGS fringe pattern are clearly presented. For the same magnitude ofK_{I}, enlarge the V-notch angle will develop the smaller CGS fringe loops. When the notch angle is large enough, the left and right lobes almost disappear and the front loops existed solely. This phenomenon lies in the rapid diminishing of deformation gradient at the left and right edge around the notch tip with larger notch angle.

(4) CGS fringes for mode I V-notch tip are experimentally investigated in three-point-bending specimen. The front loops of CGS fringe patterns at the V-notch tip show a good agreement between the experimental and theoretical contours, and the geometrical patterns of the left and right loops are not in good agreement with theoretical fringes. This is due to the notch cutout residual stresses and the variation in notch tip triaxiality with notch angle. The stress intensity factor extracted from the front loops of CGS shows a good agreement when compared to the result from the finite element analysis with the K-dominance assumption.

(5) For the same loading condition enlarge the 2β, the larger the stress intensity factor will be. But it does not imply higher stress concentration for the larger notch angle. This is due to different units of the stress intensity factor for various 2β values (for V-notch tip, the stress intensity factor is not the function of $r^{-1/2}$ but $r^{\lambda-1}$, and λ depends on the notch angle). The varying trend of stress concentration depends on the 2β value.

Acknowledgments

The research project no.10372048 is supported by NSFC, Science Foundation of Tsinghua University, Start foundation of oversea-return people in ministry of education of China.

References

Atkinson, C., Bastero, J.M., Martinez-Esnaola, J.M., 1988. Stress analysis in sharp angular notches using auxiliary fields. Engineering Fracture Mechanics 31 (67), 637–646.

Bruck, H.A., Rosakis, A.J., 1992. On the sensitivity of coherent gradient sensing. Part I. A theoretical investigation of accuracy in fracture mechanics applications. Optics and Lasers in Engineering 17 (2), 83–101.

Bruck, H.A., Rosakis, A.J., 1993. On the sensitivity of Coherent Gradient Sensing. Part II. An experimental investigation of accuracy in fracture mechanics applications. Optics and Lasers in Engineering 18 (1), 25–51.

Chen, D.H., 1995. Stress intensity factors for V-notched strip under tension or in-plane bending. International Journal of Fracture 70 (1), 81–97.

Dunn, M.L., Suwito, W., Cunningham, S.J., 1997. Fracture initiation at sharp notches: correlations using critical stress intensities. International Journal of Solids and Structures 34 (29), 3873–3883.

El-Hadek, M.A., Tippur, H.V., 2003a. Dynamic fracture parameters and constraint effects in functionally graded syntactic epoxy foams. International Journal of Solids and Structures 40 (8), 1885–1906.

El-Hadek, M.A., Tippur, H.V., 2003b. Dynamic fracture behavior of syntactic epoxy foams: optical measurements using coherent gradient sensing. Optics and Lasers in Engineering 40 (4), 353–369.

Kondo, T., Kobayashi, M., Sekine, H., 2001. Strain gage method for determining stress intensities of sharp-notched strips. Experimental Mechanics 41 (1), 1–7.

Krishnaswamy, S., Tippur, H.V., Rosakis, A.J., 1992. Measurement of transient crack tip deformation fields using the method of coherent gradient sensing. Journal of the Mechanics and Physics of Solids 40 (2), 339–372.

Lambros, J., Rosakis, A.J., 1997. Dynamic crack initiation and growth in thick unidirectional graphite/epoxy plates. Composites Science and Technology 57 (1), 55–65.

Lee, Y.J., Rosakis, A.J., Lambros, J., 1996. Analysis of coherent gradient sensing (CGS) by Fourier optics. Optics and Lasers in Engineering 25 (1), 25–53.

Mahinfalah, M., Zackery, L., 1995. Photoelastic determination of mixed mode stress intensity factors for sharp reentrant corners. Engineering Fracture Mechanics 52 (4), 639–645.

Park, T.S., Suresh, S., Rosakis, A.J., Ryu, J., 2003. Measurement of full-field curvature and geometrical instability of thin film–substrate systems through CGS interferometry. Journal of the Mechanics and Physics of Solids 51 (11), 2191–2211.

Prassianakis, J.N., Theocaris, P.S., 1990. Stress intensity factors of V-notched elastic, symmetrically loaded, plates by method of caustics. Journal of Physics D: Applied Physics 13, 1043–1053.

Rosakis, A.J., 1993. Application of coherent gradient sensing (CGS) to the investigation of dynamic fracture problems. Optics and Lasers in Engineering 19 (1), 3–41.

Rosakis, A.J., Ravi-Chandar, K., 1986. On the crack-tip stress state: an experimental evaluation of three-dimensional effects. International Journal of Solids and Structures 22 (1), 121–134.

Rosakis, A.J., Singh, R.P., Tsuji, Y., Kolawa, E., Moore Jr., N.R., 1998. Full field measurements of curvature using coherent gradient sensing: application to thin film characterization. Thin Solid Films 325 (1–2), 42–54.

Seweryn, A., Molski, K., 1996. Elastic stress singularities and corresponding generalized stress intensity factors for angular corners under various boundary conditions. Engineering Fracture Mechanics 55 (4), 529–556.

Tippur, H.V., Krishnaswamy, S., Rosakis, A.J., 1992. A coherent gradient sensor for crack tip measurements: analysis and experimental results. International Journal of Fracture 52 (1), 193–204.

Tippur, H.V., Xu, L., 1995. Measurement of interfacial fracture parameters using coherent gradient sensing (CGS). Strain 31 (1), 143–149.

Williams, M.L., 1952. Stress singularities resulting from various boundary conditions insingular corners of plates inextension. Journal of Applied mechanics 19 (3), 526–528.

Xu, W., Yao, X.F., Xu, M.Q., Jin, G.C., Yeh, H.Y., 2004. Fracture characterizations of V-notch tip in PMMA polymer material. Polymer Testing 23 (5), 509–515.

Yao, X.F., Kolstein, M.H., Bijlaard, F.S.K., Xu, W., Xu, M.Q., 2003. Tensile strength and fracture of glass fiber-reinforced plastic (GFRP) plate with an eccentrically located circular hole. Polymer Testing 22 (8), 955–963.

Yao, X.F., Xu, W., Xu, M.Q., Jin, G.C., Yeh, H.Y, 2004a. Caustic study on stress singularities in laminated composites under concentrated loads. International Journal of Solid and Structure 41 (13), 3383–3393.

Yao, X.F., Chen, J.D., Jin, G.C., Arakawa, K., Takahashi, K., 2004b. Caustic analysis of stress singularities in orthotropic composite materials with mode-I crack. Composite Science and Technology 64 (7–8), 917–924.